RESEARCH ARTICLE

3D Bioprinting of Biomimetic Bilayered Scaffold Consisting of Decellularized Extracellular Matrix and Silk Fibroin for Osteochondral Repair

Xiao Zhang†, Yang Liu†, Qiang Zuo†, Qingyun Wang, Zuxi Li, Kai Yan, Tao Yuan, Yi Zhang, Kai Shen, Rui Xie, Weimin Fan*

Department of Orthopedics, The First Affiliated Hospital of Nanjing Medical University, Nanjing, China
†*These authors contributed equally to this work*

Abstract: Recently, three-dimensional (3D) bioprinting technology is becoming an appealing approach for osteochondral repair. However, it is challenging to develop a bilayered scaffold with anisotropic structural properties to mimic a native osteochondral tissue. Herein, we developed a bioink consisting of decellularized extracellular matrix and silk fibroin to print the bilayered scaffold. The bilayered scaffold mimics the natural osteochondral tissue by controlling the composition, mechanical properties, and growth factor release in each layer of the scaffold. The *in vitro* results show that each layer of scaffolds had a suitable mechanical strength and degradation rate. Furthermore, the scaffolds encapsulating transforming growth factor-beta (TGF-β) and bone morphogenetic protein-2 (BMP-2) can act as a controlled release system and promote directed differentiation of bone marrow-derived mesenchymal stem cells. Furthermore, the *in vivo* experiments suggested that the scaffolds loaded with growth factors promoted osteochondral regeneration in the rabbit knee joint model. Consequently, the biomimetic bilayered scaffold loaded with TGF-β and BMP-2 would be a promising strategy for osteochondral repair.

Keywords: Tissue engineering; Three-dimensional bioprinting; Osteochondral repair; Extracellular matrix; Silk fibroin; Polycaprolactone

*Correspondence to: Weimin Fan, Department of Orthopaedics, The First Affiliated Hospital of Nanjing Medical University, Nanjing 210029, China; fanweimin1959@vip.sina.com

Received: July 8, 2021; **Accepted:** August 20, 2021; **Published Online:** September 14, 2021

Citation: Zhang X, Liu Y, Zuo Q, *et al.,* 2021, 3D Bioprinting of Biomimetic Bilayered Scaffold Consisting of Decellularized Extracellular Matrix and Silk Fibroin for Osteochondral Repair. *Int J Bioprint*, 7(4):401. http://doi.org/10.18063/ijb.v7i4.401

1. Introduction

Osteochondral defects, which occur due to inflammation, trauma or aging, involve lesions of cartilage and subchondral bone and constitute a significant healthcare burden[1,2]. Current treatment strategies include microfracture, autologous chondrocyte implantation, and mosaicplasty. Nonetheless, there are still failures and undesirable complications in the above-mentioned treatment strategies[3-6]. In recent years, tissue engineering that provides suitable biomaterials to support the growth and differentiation of cells provides a promising strategy for osteochondral regeneration[7,8]. The application of bilayered scaffolds that concerned physical structure of osteochondral tissue has been the focus of osteochondral regeneration research[9,10]. Ideal bilayered scaffolds should be equipped with biological and physical properties that can match the native tissues[11,12]. However, traditional tissue engineering strategies have not been able to develop a bilayered scaffold with anisotropic structural properties to mimic a native osteochondral tissue[13]. Furthermore, each layer of the current bilayered scaffolds is usually fabricated separately and then joined together, resulting in a poor integration between two layers of the bilayered construction[11,14,15]. Recently, 3D bioprinting has emerged as a continuous way to fabricate biomimetic and complex tissue structure, such as osteochondral bilayered structure[11,13,16]. Three-dimensional (3D) bioprinting technology integrates equipment manufacturing industry, biomaterial science, and computer aided to fabricate

© 2021 Zhang, *et al*. This is an Open Access article distributed under the terms of the Creative Commons Attribution License, permitting distribution and reproduction in any medium, provided the original work is cited.

"living" engineered tissue or organ using bioink containing living cells, and thus has great potential in regeneration medicine[17-20].

3D bioprinting techniques can be classified into three distinct process categories: (i) Material extrusion[21], (ii) material jetting[22], and (iii) vat polymerization bioprinting[23]. Of these, extrusion-based bioprinting is the most prevalent employed research approach to fabricate 3D cell-laden scaffolds due to its accessibility, cost-effectiveness, and capacity to replicate tissue complexity[21]. For extrusion-based bioprinting, various biomaterials, such as gelatin, HA, or alginate, have been extensively used as bioink sources[24-28]. However, some problems remain, such as the cell toxicity of the chemical cross-link process, poor cell-material interactions, and inferior tissue formation[29,30]. In addition, only a small percentage of cells in these materials could drive cell differentiation towards target cell lineage[30,31]. Moreover, these materials cannot represent the complexity of extracellular matrices of repaired natural tissue. Therefore, there is an urgent need to develop a bioink that is sufficient to create a tissue-specific microenvironment with 3D cellular organization and cell-to-cell/cell-to-matrix communication that are typical of natural tissues.

Decellularized extracellular matrix (dECM) has been developed as bioink to fabricate 3D bioprinted tissues and organs[32,33]. Both biologically and functionally, dECM is more representative of the natural extracellular matrix (nECM) than other kinds of biomaterials. dECM provides a native-mimicking microenvironment for the migration, proliferation, and differentiation of bone marrow-derived mesenchymal stem cells (BMSCs)[34,35]. Furthermore, BMSCs encapsulated in cartilage dECM (DCM) or bone dECM (DBM) hydrogel can recognize and interact with surrounding matrix that specifically enhanced chondrogenic/osteogenic differentiation and tissue maturation[36]. However, the mechanical strength of DCM and DBM is insufficient because of the loss of cartilage/bone native tissue structure during the homogenization and solubilization process[36,37]. Silk fibroin (SF) is a natural biopolymer that is widely investigated for various 3D bioprinting and tissue engineering applications due to its remarkable mechanical properties, biocompatibility and biodegradation nature[38,39]. In our previous study, we reported the use of a cross-linker-free DCM-SF bioink in printing 3D construct which had similar mechanical properties compared with native cartilage tissue[37].

Since dECM-based bioink most likely retain endogenous growth factors than other kinds of bioink, it will lead to enhancement of osteochondral regeneration that incorporates additional exogenous growth factors in dECM bioink. The previous studies have shown that dECM acts as an excellent growth factor delivery system since the extracellular matrix (ECM) itself is a natural reservoir for growth factors which have a natural affinity to ECM[40,41]. Transforming growth factor-beta (TGF-β) is regarded as a highly efficient chondrogenic factor[42]. Bone morphogenetic protein-2 (BMP-2) plays a key role in driving osteogenesis of BMSCs[43]. Hence, the combination of such a bioink with TGF-β and BMP-2 is effective to enhance osteochondral regeneration.

Therefore, on the basis of our previous study, we employed dECM-SF bioink to fabricate 3D-printed bilayered constructs. First, polycaprolactone (PCL) was first extruded to print frame of bone layer, and the DBM bioink was printed to fill the space. The DCM bioink was used to print the cartilage layer on the bone layer. Next, we evaluated the mechanical strength and degradation rate of the two layers to confirm the properties of constructs. Furthermore, the delivery capacity of growth factors and the potential of constructs for chondrogenesis or osteogenesis were measured *in vitro*. Finally, we implanted bilayered constructs containing TGF-β1 and BMP-2 into the osteochondral defect and determined the osteochondral regeneration efficacy *in vivo*.

2. Materials and methods

All experimental procedures involving animals have been approved and implemented in accordance with the animal use guidelines outlined by the Medical College of Nanjing Medical University (IACUC-2005033). All animal subjects were treated in accordance with the National Laboratory guidelines for Laboratory Animal Nursing.

2.1. Preparation of decellularized cartilage/bone ECM

Decellularized DCM and DBM were prepared based on our previously reported method[37]. Briefly, articular cartilage and cancellous bone segments were harvested from female goats (n = 12) within 6 h after sacrifice. These cartilage and bone segments were washed, freeze-dried, and immersed in liquid nitrogen and cut into small pieces (1~2 mm^3). The cartilage pieces were rinsed with phosphate-buffered saline (PBS), while the bone pieces were demineralized using an adaptation of previously reported methods by submerging in 0.5 M hydrochloric (HCL) under agitation for 24 h, and then degreased with 1:1 mixture of chloroform and methanol for 2–3 h[44]. Cartilage and demineralized bone pieces were washed thoroughly with PBS and lyophilized before decellularization. The cartilage and bone pieces were homogenized, milled, and soaked in PBS containing 0.1% w/v ethylenediaminetetraacetic acid (EDTA; Sigma-Aldrich, St. Louis, MO, USA) and 3.5% w/v phenylmethyl sulfonylfluoride (PMSF; Beyotime, Shanghai, China) for 24 h to inhibit protease activity. These cartilage and bone granules were treated with a 1%

solution of Triton X-100 in a protease inhibitor cocktail (0.1% w/v EDTA, 3.5% w/v PMSF in Tris-HCl, pH = 7.5) for 24 h. Next, the cartilage and bone granules were washed and digested with 50 U/mL deoxyribonuclease and 1 U/mL ribonuclease (Sigma-Aldrich, St. Louis, MO, USA) for 12 h. To obtain DCM and DBM, the granules were lyophilized and solubilized using a previously reported protocol with modifications[30]. In brief, 10 mg decellularized granules were mixed with 1 mL of 0.1 mol HCl containing 1 mg of pepsin powder (Sigma-Aldrich, St. Louis, MO, USA) at room temperature for 2 days. After solubilization, 1 Mol NaOH was added to adjust the pH to 7.4. The solution was centrifuged at 10,000 ×*g* for 3 min to remove undigested particles and the supernatant was lyophilized and stored at −80℃ for longer storage.

2.2. Preparation of TGF-β1-loaded DCM/SF bioink

Solubilized and lyophilized SF protein (SF, molecular weight >100 kDa) was purchased from Simatech Inc. (Suzhou, China). Polyethylene glycol (PEG 400; molecular weight 380~420 Da) was provided by Aladdin Inc. (Shanghai, China). About 10% w/v of SF, 5% w/v DCM, and 4 μg/mL of TGF-β1 (PeproTech, Rocky Hill, USA) were dissolved in PBS to prepare SF/DCM blends. The blends were then mixed with an equal volume of 80% v/v PEG for gelation of the DCM/SF bioinks (5% w/v final SF concentration; 2.5% w/v final DCM concentration; and 2 μg/mL final TGF-β1 concentration).

2.3. Preparation of BMP-2-loaded DBM/SF bioink

About 10% w/v of SF, 5% w/v DBM, and 4 μg/mL of BMP-2 (PeproTech, Rocky Hill, USA) were dissolved in PBS to prepare SF/DBM blends. The blends were then mixed with an equal volume of 80% PEG for gelation of the DBM/SF bioinks (5% w/v final SF concentration; 2.5% w/v final DBM concentration; and 2 μg/mL final BMP-2 concentration).

2.4. Cell isolation and encapsulation

BMSCs were harvested and isolated as we previously described[45,46]. Briefly, bone marrow aspirate was isolated from the medullary cavity of femur bone in New Zealand rabbits. The mixture of cells was separated by gradient density centrifugation in 1.073 g/ml lymphocyte separation solution (Gibco, NY, USA). The mononuclear fraction interphase was collected and washed twice in sterile PBS. The cells were resuspended in low-glucose DMEM containing 100 U/ml penicillin, 100 U/ml streptomycin, and 10% fetal bovine serum (HyClone, UT, USA), and subsequently incubated at 37°C with 5% CO_2. The culture medium was changed to remove suspension cells after 48 h, and the adherent cells were expanded up to passage 3. To encapsulate cells for 3D bioprinting, BMSCs were trypsinized after reaching approximately 80% confluence and then washed with low-glucose DMEM containing 10% fetal bovine serum. After centrifugation at 1200 rpm for 5 min, BMSCs were resuspended in bioinks at a density of 1.0×10^7 cells mL^{-1}.

2.5. Fabrication of bilayered scaffolds

3D bioprinting system (3D Discovery, Regenhu, Villaz-St-Pierre, Switzerland) provided by Bioexcellence Inc. (Beijing, China) was used to fabricate the bilayered scaffolds. DBM bioink and DCM bioink were prepared and loaded into 10 mL plastic containers at room temperature. FDA-approved PCL (molecular weight 70–90 Kda) provided by Polysciences Inc. (PA, USA) was loaded into metal container with temperature control, and the container temperature was set to 60°C. The parameters related to the process of printing are listed in **Table 1**.

For the fabrication of the bone layer (4 mm in diameter, 4.5 mm in height), PCL was first extruded to print outline, and then, the DBM/SF bioink was printed to fill the space. DCM/SF bioink was used to print the cartilage layer (4 mm in diameter, 0.5 mm in height) on the bone layer (**Figure 1**). The thicknesses of cartilage layer and bone layer were adjusted to 2 mm for *in vitro* investigation.

2.6. Fourier-transform infrared (FTIR) spectroscopy

The infrared spectra of DCM/SF and DBM/SF hydrogels were evaluated using Thermo Scientific Nicolet iS5 FT-IR Microscope (Waltham, MA, USA). The samples were prepared by lyophilization for FTIR analysis. Scanning was conducted in the spectral range from 1000 cm^{-1} to 2200 cm^{-1}.

Table 1. Parameters of the designed construct and 3D bioprinting.

Parameters	Cartilage layer	Bone layer	
	DCM/SF bioink	DBM/SF bioink	PCL
Container temperature	**15°C**	**15°C**	**60°C**
Nozzle diameter	0.25 mm	0.25 mm	0.25 mm
Size (length * width * height)	4 mm* 4 mm*0.5 mm	4 mm*4 mm*4.5 mm	
Interlayer spacing	0.25 mm	0.25 mm	0.25 mm
Line spacing	0.20 mm	0.20 mm	2 mm
Printing speed	4 – 7 mm/s	3 – 5 mm/s	1.8 ~ 2.7 mm/s
Print pressure	0.20–0.30 MPa	0.20 – 0.30 MPa	0.50~0.60 MPa

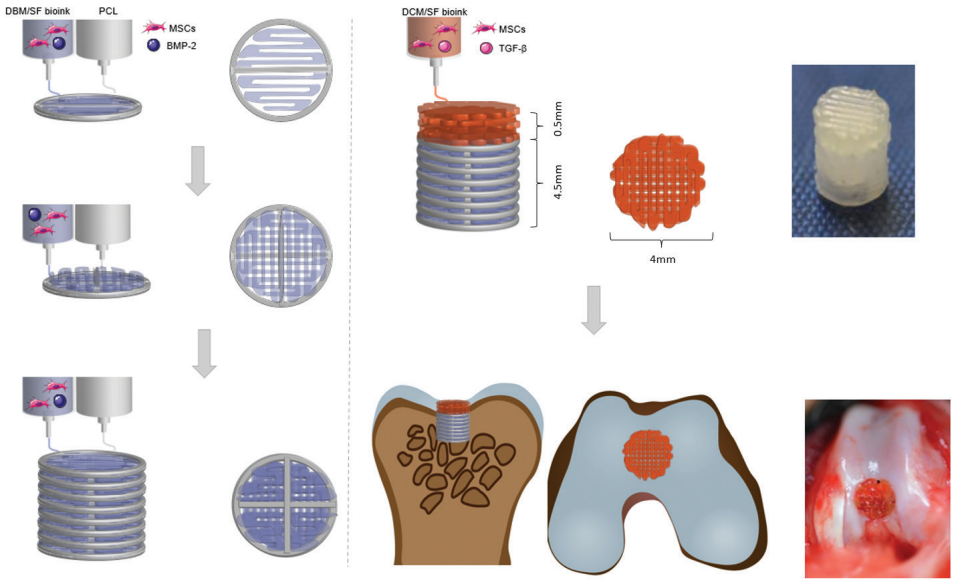

Figure 1. Schematic illustration of the bilayered scaffold loaded with transforming growth factor-β and bone morphogenetic protein-2 for osteochondral repair.

2.7. Rheological analysis

Thermo Scientific HAAKE MARS 40 Rheometer (Waltham, MA, USA) was used to investigate rheological properties fitted with 25 mm parallel geometry. Frequency-dependent loss modulus (G''), storage modulus (G'), and dynamic viscosity of DCM/SF and DBM/SF hydrogels were determined by the frequency sweep in the shear rate range of 0.1~100 Hz at 15℃.

2.8. Growth factor releasing

To investigate release of growth factors, cartilage layer and bone layer construct samples were encapsulated with 2 μg/mL TGF-β1 and 2 μg/mL BMP-2, respectively. To evaluate the release rate of TGF-β1, pre-weighed cartilage layer samples were rinsed with 2 ml PBS solutions containing 0.05% EDTA, 0.1% heparin, 0.02% sodium azide, and 0.1% BSA at 37°C. The PBS solution was replenished and harvested every 48 h for 21 days. The harvested PBS samples were then assessed by TGF-β1 ELISA Kit assay (PeproTech, RH, USA). To evaluate the release rate of BMP-2, pre-weighed bone layer samples were rinsed with 2 ml PBS solutions containing 0.05% EDTA, 0.1% heparin, 0.02% sodium azide, and 0.1% BSA at 37°C. The PBS solution was replenished and harvested every 48 h for 14 days. The harvested PBS samples were then assessed by BMP-2 ELISA Kit assay (PeproTech, Rocky Hill, USA). All samples were analyzed in triplicate.

2.9. Cell viability

For the observation of cell viability, LIVE/DEAD cell staining kit (Molecular Probes, OR, USA) was used to stain cells. Cell-scaffold construct samples were incubated in low-glucose DMEM containing 2 μM calcein AM (live) and 4 μM ethidium homodimer-1 (dead) reagents at 37°C for 45 min. Fluorescence images were obtained from a fluorescence microscope (Zeiss, Nanjing, China). Calcein AM (green) and ethidium homodimer-1 (red) were detected by excitation wavelengths of 495 nm and 560 nm, respectively. The cell survival rate at 1 and 3 days was analyzed using ImageJ software. Cell proliferation and viability in construct samples were examined using CCK8 assay (Beyotime, Nanjing, China) after 1, 4, and 7 days of culture.

2.10. Degradation of 3D bilayered scaffolds

For the analysis of degradation of bilayered scaffolds, the rates of weight loss were performed with treatment of protease XIV enzyme at several time points over 24 days. The weight loss test of cartilage layer and bone layer was conducted separately. The initial dry printed scaffold was weighed as W0 and the enzyme solution was changed every day. Scaffolds were taken out from the enzyme solution and weighed at dry state at each time point (Wd). The degradation rate was defined as $100\% \times (W0 - Wd)/W0$.

2.11. Comprehensive stress

For the investigation of comprehensive properties, cartilage layer and bone layer construct samples were loaded on an Instron Tensile Force Tester (Instron, HW, UK). A displacement rate of 0.1 mm/min was set to obtain stress-strain curve. The compression modulus was determined from the linear region of the stress-strain curve.

2.12. mRNA expression

For mRNA expression analysis, cell-scaffold construct samples were cultured for 7 and 14 days (n = 3). For mRNA extraction, the samples were homogenized and lysed in TRIzol (Yeasen, Shanghai, China) before being centrifuged at 12,000 rpm at 4°C. Subsequently, a cDNA reverse transcription kit (Yeasen, Shanghai, China) was used to reverse-transcribed total RNA into cDNA. The expression levels of cartilage-related markers (COL II, type-2 collagen; ACAN, aggrecan; SOX-9, SRY-box transcription factor 9) and osteogenic-related markers (COL I, type-1 collagen; OCN, osteocalcin; ALP, alkaline phosphatase; RNUX2, runt-related transcription factor 2) were analyzed by real-time qPCR system (Applied Biosystems, CA, USA). The target mRNA was normalized to a housekeeping control (glyceraldehyde 3-phosphate dehydrogenase mRNA) and determined using the ΔΔCt method. The sequences are listed in **Table S1**.

2.13. *In vivo* surgical operation

To determine the osteochondral regeneration effect *in vivo*, New Zealand white rabbits weighted 2.0 – 3.0 kg were chosen to create osteochondral defect models. After general anesthesia, osteochondral defects (diameter: 4 mm, depth: 5 mm) were caused on the patellar groove of right knee joints. In the control group (n = 6), the defect was left blank without material added. In the pristine-bilayered construct group (PB group) (n = 6), the constructs without bioactive growth factors were implanted into the defects. In the GF-bilayered construct group (GB group) (n = 6), bilayered constructs containing TGF-β1 and BMP-2 were implanted in the osteochondral defect (**Figure S2A and B**). The rabbits were anesthetized and executed 3 months after operation.

2.14. Histological and immunohistochemical analysis

For histological assessment, rabbit femurs were fixed overnight in 4% paraformaldehyde at 4°C and then decalcified with decalcification solution for about 30 days. The decalcified constructs were dehydrated with a graded series of ethanol and embedded in paraffin for sectioning. The deparaffinized paraffin sections were stained with safranin O and Masson's trichrome, and imaged with an Olympus microscope. To further observe the expression of COL II and OCN, immunohistochemical staining was performed as we previously described[47]. The ICRS Visual Histological Assessment Scale was carried out to score the morphology and the degree of metachromatic staining, respectively. The total score ranged from 0 to 18, including semi-quantitative scales to rate the surface, matrix, cell distribution, viability of the cell population, subchondral bone, and cartilage mineralization.

2.15. Biochemical analysis

We analyzed the contents of collagen and sulfated-glycosaminoglycan (sGAG) of samples. Samples were dissolved in papain digestion (125 μL/mL papain, 100 mM EDTA, and 5 mM L-cysteine; Sigma-Aldrich, MO, USA) at pH 6.5 at 60°C under rotation for 18 h. Collagen content was examined by quantifying hydroxyproline concentration. Briefly, the hydroxyproline content of the solution was determined by the chloramine-T assay after acidic hydrolyzation in 38% HCl for 18 h at 110°C. Collagen content was calculated by assuming a hydroxyproline: collagen ratio of 1:7.69. The total sGAG content was analyzed by the 1,9-dimethylmethylene blue (DMMB; Sigma-Aldrich, MO, USA) assay. The sGAG and collagen content were normalized by dry weight of construct.

2.16. Statistical analysis

All data are expressed as the mean ± standard deviation (SD), and $P < 0.05$ was considered statistically significant. For statistical analysis, intergroup differences were calculated by analysis of variance (ANOVA) after testing for homogeneity of variance. All statistical analysis was performed using Statistical Package for the Social Sciences (SPSS) version 19.0 software (IBM SPSS Statistics for Windows, Armonk, NY, USA).

3. Results and discussion

3.1. Preparation and characterization of DCM/SF and DBM/SF bioinks

To estimate the ECM component change, we determined the collagen and glycosaminoglycans (GAGs) contents before and after decellularization (**Figure S1A and B**). A significant loss of collagen and GAGs in DCM and DBM was observed after decellularization. The reason behind the reduction of the collagen and GAGs is the treatment with the enzymes during the trypsinization and decellularization including deoxyribonuclease , ribonuclease and pepsin[30,48]. Quantification of DNA content from native ECM (NCM and NBM) and dECM (DCM and DBM) revealed the significant reduction (~96%) in the case of dECM as compared to the native ECM before decellularization.

We investigated rheological behavior to explore flow properties of DCM/SF and DBM/SF bioinks. The frequency sweep indicated that viscosity of DCM/SF and DBM/SF bioinks decreased in response to linearly increasing shear rate (**Figure 2A**), indicated that the bioinks exhibited shear-thinning flow behavior, which are similar to most polymer gels[36]. Furthermore, the G' values exceeded the G'' values over the whole angular frequency range (G' > G''; **Figure 2B**), indicating the formation of a typical gel structure[49].

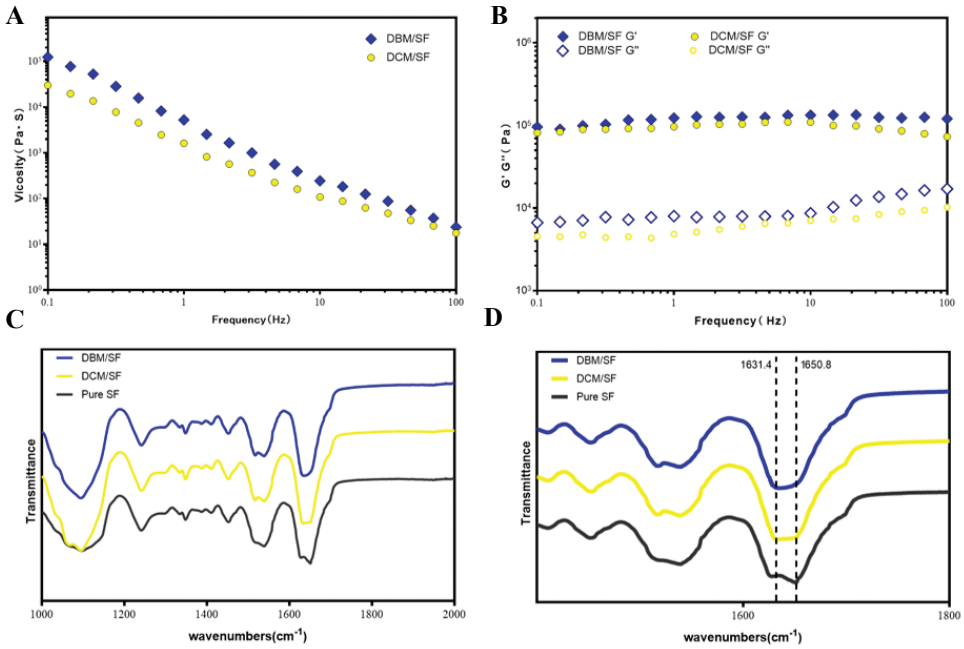

Figure 2. (A) Frequency sweep of the DCM/SF and DBM/SF bioinks. (B) Dynamic viscosity measurement of the DCM/SF and DBM/SF bioinks. (C, D) FTIR absorption spectra of the DCM/SF and DBM/SF bioinks.

FTIR spectroscopy was done to analyze the crystallization of SF in DCM/SF and DBM/SF bioinks (**Figure 2C**). The pure SF control group showed a major peak at 1,650.8 cm^{-1} in the amide I region (C=O stretch), suggesting the presence of a higher proportion of random coils than β-sheet structure[50]. The major peak of DCM/SF and DBM/SF bioinks in the amide-I region shifted to a lower wavelength at 1628–1632 cm^{-1} (**Figure 2D**), indicating that the mixture was dominated by β-sheet structure[51].

3.2. One-step 3D-bioprinting and characterization of a bilayered scaffolds

We printed the bilayered scaffolds as shown in **Figure 3A**. PCL was first extruded to print frame of bone layer, and the DBM bioink was printed to fill the space. The DCM bioink was used to print the cartilage layer on the bone layer. The PCL frame not only provided a mechanical support in the bone layer but it is also favorable for the cell migration and exchange of nutrients because the DCM/SF hydrogel take up more space than PCL frame in the bone layer.

For the analysis of degradation of bilayered scaffolds, the rates of weight loss were performed with treatment of protease XIV enzyme at several time points over 24 days (**Figure 3B**). Bone layer constructs showed a significantly lower degradation rate than cartilage layer constructs. The reason lies in the slow degradation characteristics of PCL frame in the bone layer. For measurement of compressive strength, 3D-printed constructs were subjected to mechanical tests. We performed the stress-strain curve to investigate the relation between compressive stress and strain (**Figure 3C**). The compressive stress finally reached the maximum before yielding for bone layer construct, bone layer construct without PCL frame, and cartilage layer construct at the compressive stress of 310 kpa, 47 kPa, and 44 kPa, respectively. The compressive modulus was significantly higher in bone layer construct than in the bone layer construct without PCL and cartilage construct, with about 9-fold enhancement (**Figure 3D**). Ding *et al*. reported that the difference in compressive modulus is approximately 5–20 times between natural cartilage and bone[52].

We then observed the viability of BMSCs in printed cartilage and bone layers by live/dead staining assay (**Figure 4A and B**). The survival rates of BMSCs in the printed cartilage and bone layer were over 80% (**Figure 5C**). CCK8 cell proliferation assay was also carried out to ascertain the viability of BMSCs in both layers at different time points (**Figure 5D**). The optical density (OD) value increased over the 7 days of culture and did not differ significantly between cartilage and bone layer. The results indicated that the cartilage and bone layers promoted the proliferation of BMSCs and exhibited low cytotoxicity.

3.3. Release of growth factors from the scaffolds promoted differentiation of BMSCs *in vitro*

Growth factors such as TGF-β and BMP-2 play an important role in promoting directed differentiation of

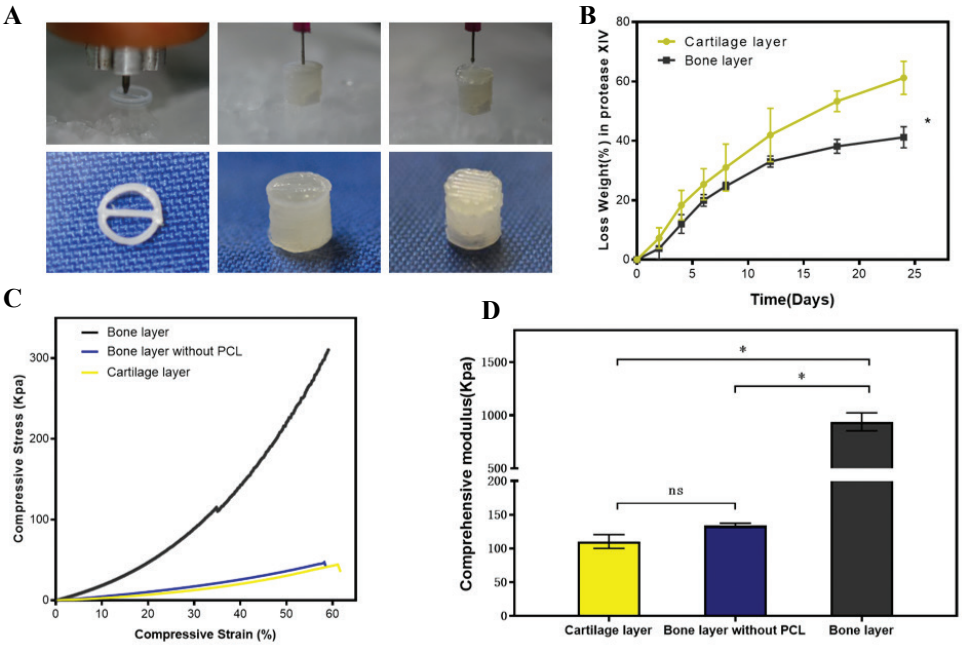

Figure 3. (A) PCL was first extruded to print frame of bone layer, and the DBM bioink was printed to fill the space. The DCM bioink was used to print the cartilage layer on the bone layer. (B) Degradation rate of cartilage layer and bone layer in protease XIV. (C) Stress-strain curve that was used to investigate the relation between compressive stress and strain. (D) Comprehensive modulus calculated by linear region of the stress-strain curve ($n = 3$; $^*P < 0.05$).

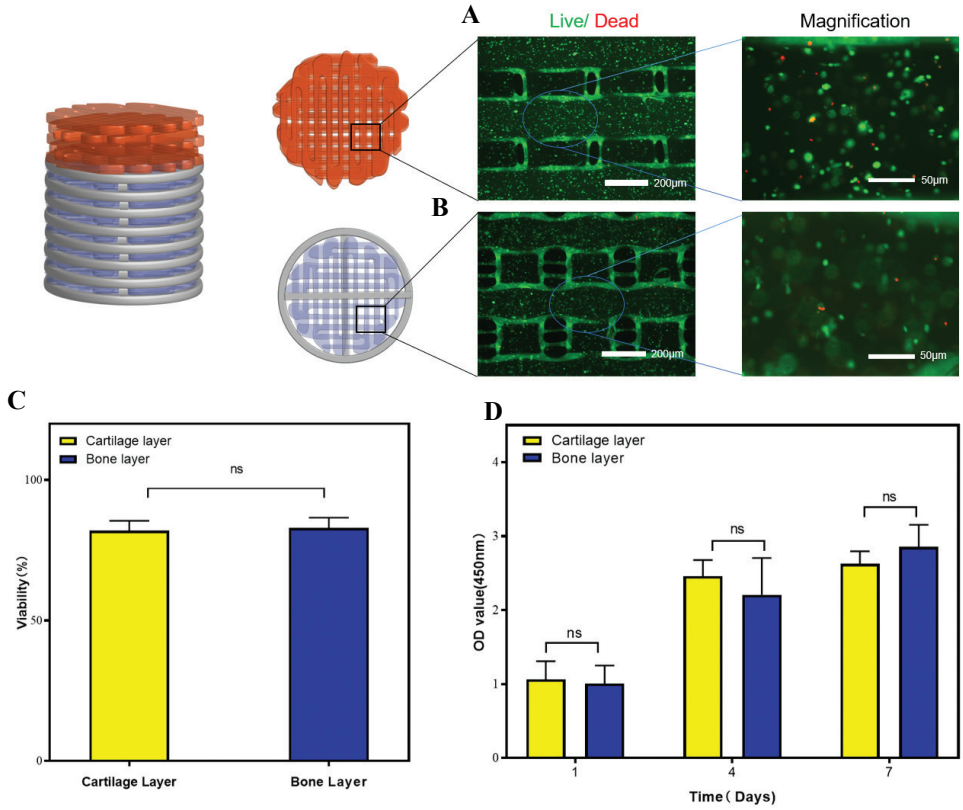

Figure 4. Viability of BMSCs in the printed constructs. Fluorescence microscopy findings of the LIVE/DEAD assay of BMSCs cultured in the (A) cartilage layer and (B) bone layer. (C) Quantification of cell viability. (D) Cell viability results obtained by the CCK-8 assay on 1, 4, and 7 days of cell culture ($n = 3$; $^*P < 0.05$).

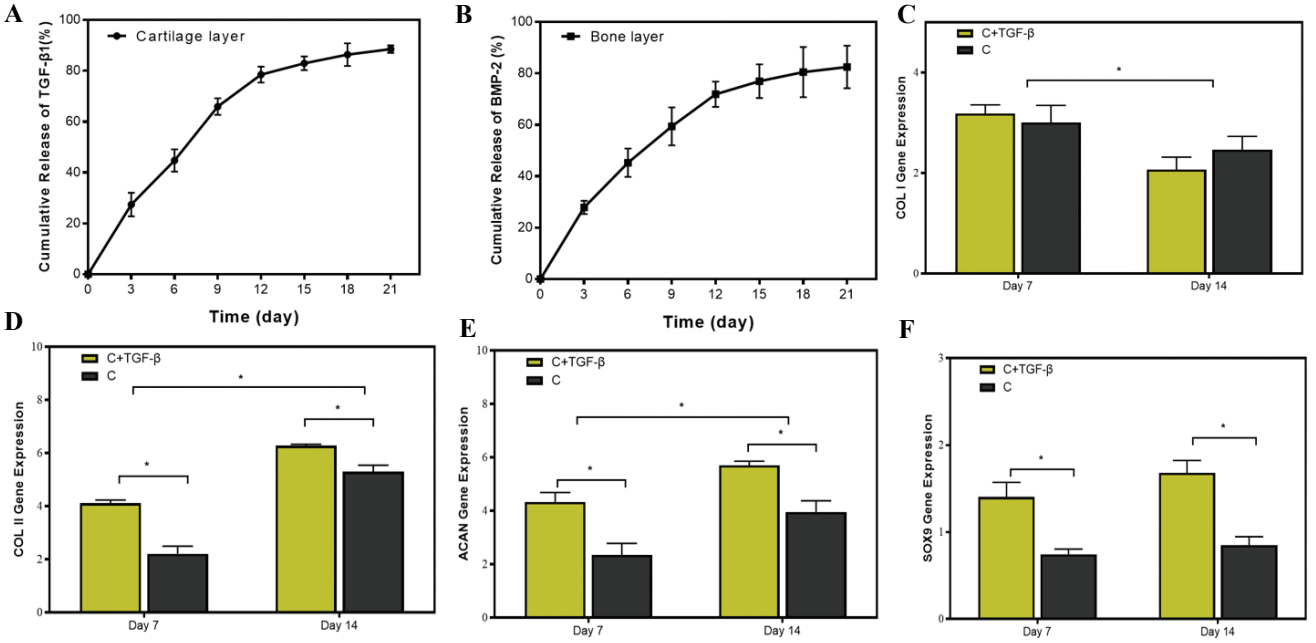

Figure 5. (A) Release kinetics of TGF-β1 from printed cartilage layer. (A) Release kinetics of TGF-β1 from printed cartilage layer. (B) Release kinetics of BMP-2 from printed bone layer. mRNA expression level of cartilage-related genes, including (C) collagen type I (*COL I*, a fibrotic marker gene), (D) collagen type II (*COL II*), (E) aggrecan (*ACAN*), and (F) *SOX-9* in cartilage layer group (C group) and cartilage layer loaded with TGF-β1 group (C+TGF-β group) on days 7 and 14 ($n = 3$; $^*P < 0.05$).

BMSCs[53,54]. Although dECM-based bioink most likely retain endogenous growth factors than other kinds of bioink, the pure dECM is always insufficient for the effective treatment of osteochondral defects due to the loss of bioactive factors during decellularized process. Datta *et al*. reported the reduction of BMP-2 in decellularized bone matrix due to decellularization[55]. Almeida *et al*. reported that the addition of exogenous TGF-β in dECM promoted the chondrogenesis of fat pad-derived stromal cells[41]. Moreover, the previous studies have shown that dECM acts as an excellent growth factor delivery system since the ECM itself is a natural reservoir for growth factors which have a natural affinity to ECM[40,41]. In this study, we developed a controlled release system by encapsulating TGF-β1 and BMP-2 into the bilayered construct.

We evaluated the TGF-β1 and BMP-2 release using ELISA to determine the capacity of scaffolds to support the controlled release of growth factors. The printed cartilage layer suggested a relatively fast release of TGF-β1 about 65.91 ± 3.29% in the beginning 9 days, with a slow release reached to 88.51 ± 1.51 % in the following days (**Figure 5A**). BMP-2 in the printed bone layer displayed an initial burst release to 59.39 ± 7.36% within the first 9 days (**Figure 5B**). BMP-2 exhibited a sustained release profile after being released for more than 12 days. The cumulative release of BMP-2 reached to 82.45 ± 8.26% after being released for 21 days. The results indicated that the bilayered construct exhibited sustained long-term release of growth factors.

Next, we investigated whether the release of TGF-β has an effect on chondrogenic differentiation potential of BMSCs in cartilage layer *in vitro*. To answer this question, we examined the mRNA expression levels of collagen I (COL I), collagen II (COL II), aggrecan (ACAN), and SOX-9 by real-time quantitative polymerase chain reaction (qPCR) on days 7 and 14 of culture (**Figure 5C-F**). The reverse transcription polymerase chain reaction (RT-PCR) analysis showed that the mRNA expression levels of COL I in C+TGF-β group were comparable to that in C group. The mRNA expression levels of COL I were significantly decreased from day 7 to day 14. The expression of COL II and ACAN in the C+TGF-β group was significantly higher than that in the C group at 2 time points. In addition, the expressions of COL II and ACAN in the C+TGF-β group and C group at day 14 were significantly increased as compared with day 7. SOX-9, a member of the Sry-type HMG box (SOX) gene family, is expressed to activate the expression of cartilage ECM-related gene (COL II and ACAN) and suppress the expression of fibrotic-related gene (COL I)[56]. SOX-9 plays a key role in the chondrogenic differentiation process of stem cells. The previous studies reported that SOX-9 is activated during very early events in chondrogenesis of BMSCs, and directly or indirectly maintains its regulation during the differentiation and maturation of chondrocytes[57]. The RT-PCR analysis showed that the SOX-9 transcription level was similar at the 2 time points. Significantly higher SOX-9 transcription occurred in the C+TGF-β group

than in the C group, suggesting that a higher extent of signaling cascade was activated during the chondrogenic differentiation of BMSCs over the C+TGF-β group than C group.

Furthermore, to investigate the osteogenic differentiation of BMSCs in the bone layer, the expression levels of COL I, RUNX2, OCN, and ALP were measured by RT-PCR (**Figure 6A-D**). The result showed that mRNA expression levels of COL I, RUNX2, and OCN for B+BMP-2 group were obviously higher than those for B group after culture for 14 days. The mRNA expression levels of ALP did not differ significantly between the B+BMP-2 group and the B group at day 7. On the other hand, the expression of ALP in the B+BMP-2 group was significantly higher than that in the B group at day 14. As a transcription factor, RUNX2 is expressed to activate the expression of bone-related gene (COL I, OCN, and ALP). The activation and expression of RUNX2 peak in the early stage of osteogenic differentiation of BMSCs[11]. The RT-PCR suggested that the RUNX2 expression level showed no significantly difference at the 2 time points. Meanwhile, the RUNX2 transcription level was significantly higher in the B+BMP-2 group than in the B group at days 7 and 14, indicating that a higher extent of signaling cascade was activated during the osteogenic differentiation of BMSCs in the B+BMP-2 group than in the B group. The result indicated that the B+BMP-2 constructs were able to enhance osteoinductive abilities *in vitro*.

3.4. The scaffolds loaded with growth factors promoted osteochondral regeneration *in vivo*

To investigate whether the composite constructs stimulate osteochondral regeneration *in vivo*, regenerative efficacy was further observed in a rabbit osteochondral defect model. No deaths occurred during the whole observational period. The grafts were sampled 3 months after operation. The gross macroscopic observations suggested that the regenerated tissues of the PB and GB groups seemed smooth and similar to the surrounding normal tissues (**Figure 7A**). The defects of the PB and GB groups were completely covered with excellent integration, whereas the repaired tissues of the control group only partially filled the defect and showed incomplete integration with the native cartilage tissues.

Histological and immunohistochemical staining analyses were conducted to evaluate repair efficacy. Compared to the control group and PB group, the GB group had smoother and more homogeneous neocartilage which had a considerable number of typical cartilage lacunae structures (**Figure 7B**). The cells in neocartilage of GB group were in a typical linear arrangement and similar to normal chondrocytes. Masson (blue staining) and safranin O (red staining) staining were carried out to evaluate the proportion of collagen and proteoglycan content, respectively (**Figure 7C and D**). Compared to other groups, the collagen and proteoglycan deposition in the neocartilage of GB group was abundant and uniform.

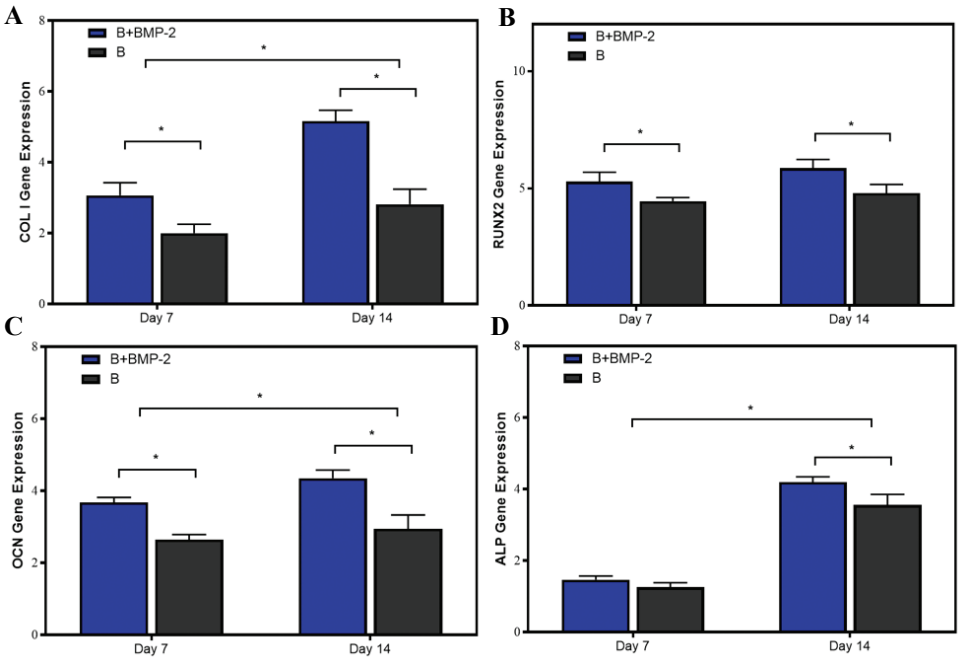

Figure 6. mRNA expression level of bone-related genes, including (A) collagen type I (*COL I*, a fibrotic marker gene), (B) RUNX family transcription factor 2 (*RUNX2*), (C) osteocalcin (*OCN*), and (D) alkaline phosphatase (*ALP*) in bone layer group (B group) and cartilage layer loaded with BMP-2 group (B+BMP-2 group) on days 7 and 14 ($n = 3$; $*P < 0.05$).

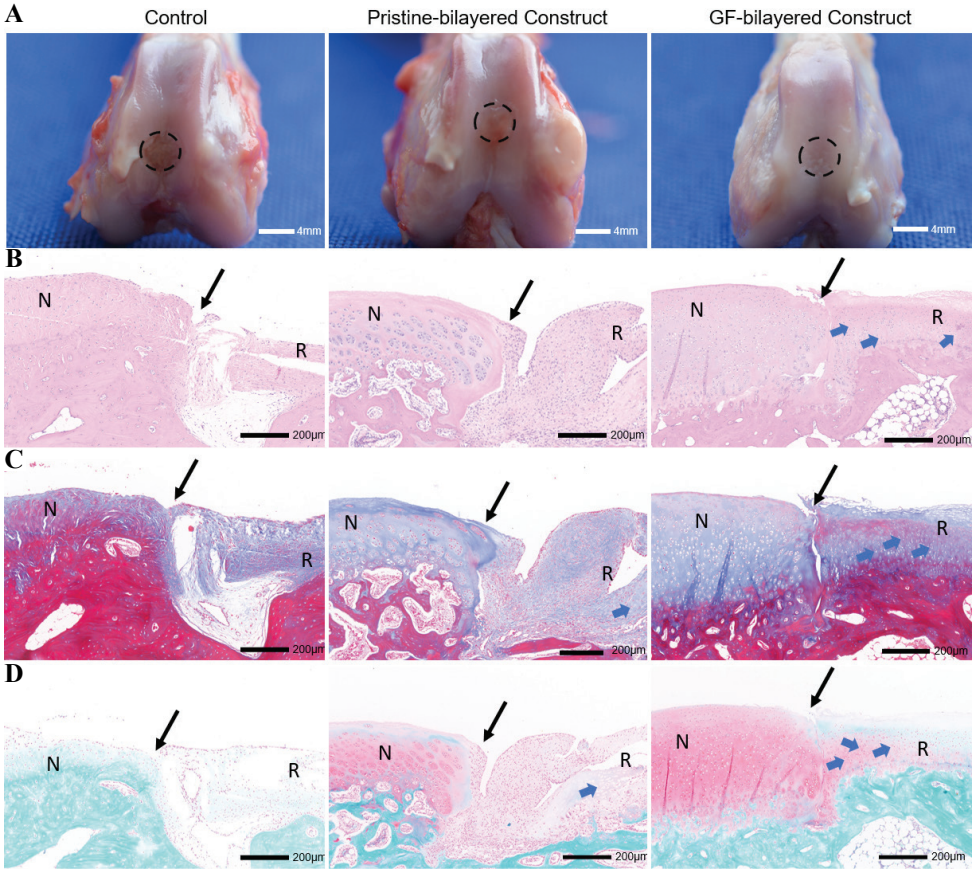

Figure 7. The bilayered constructs facilitated the regeneration of osteochondral tissues *in vivo* (n = 6). The grafts were sampled 3 months after operation. (A) Gross observations of defect repair at 3 months for the control group, pristine-bilayered construct group, and GF-bilayered construct group (scale bar: 4 mm). (B) Hematoxylin and eosin (H & E) staining of repaired cartilage at 3 months (N, normal cartilage; R, repair cartilage; blue arrows, typical cartilage lacunae structures; black arrows, the repair boundary of the cartilage surface; scale bar: 200 μm). (C) Masson staining of repaired cartilage at 3 months (scale bar: 200 μm). (D) Safranin-O/fast green staining of repaired cartilage at 3 months (scale bar: 200 μm).

Coll II immunohistochemical staining demonstrated more intense staining in the GB group compared to other two groups (**Figure 8A**). A high expression of Coll II surrounding the chondrocytes could be observed in the neocartilage of GB group. Neovascularization, trabecula structure (**Figure 8B and C**), and higher intensity of staining of OCN **(Figure 8D)** could be observed in the neo-bone of GB group. While in the control group, incompletely calcified cancellous bone could be found in the bone layer. Furthermore, we performed a histologic score according to the ICRS Visual Histological Assessment Scale (**Figure S2C**). The histologic score was significantly higher in the GB group than in the PB and control groups.

Regenerated cartilage was further investigated by quantifying sGAG and collagen contents. The sGAG content of neocartilage was 9.36 ± 1.279 μg/mg in control group, 16.03 ± 0.784 μg/mg in PB group, and 24.83 ± 1.866μg/mg in GB group, with statistically significant differences ($P < 0.05$). The collagen content of neocartilage was 72.95 ± 5.82 μg/mg in control group, 106.50 ± 7.84 μg/mg in PB group, and 115.50 ± 11.28 μg/mg in GB group. The collagen content of GB group and PB group was significantly higher than that of control group. There was no significant difference between collagen content in the GB group and PB group.

In the current study, we demonstrated that a 3D bioprinted bilayered scaffolds can be used as a controlled released system, which leads to the reconstruction of osteochondral tissue. Each layer of bilayered scaffolds had a suitable mechanical strength and degradation rate. Furthermore, the scaffolds encapsulating TGF-β1 and BMP-2 can act as a controlled release system and promote osteochondral regeneration. Although the mechanical strength of the bilayered scaffolds needs to be further enhanced, this method does provide a novel strategy for osteochondral regeneration.

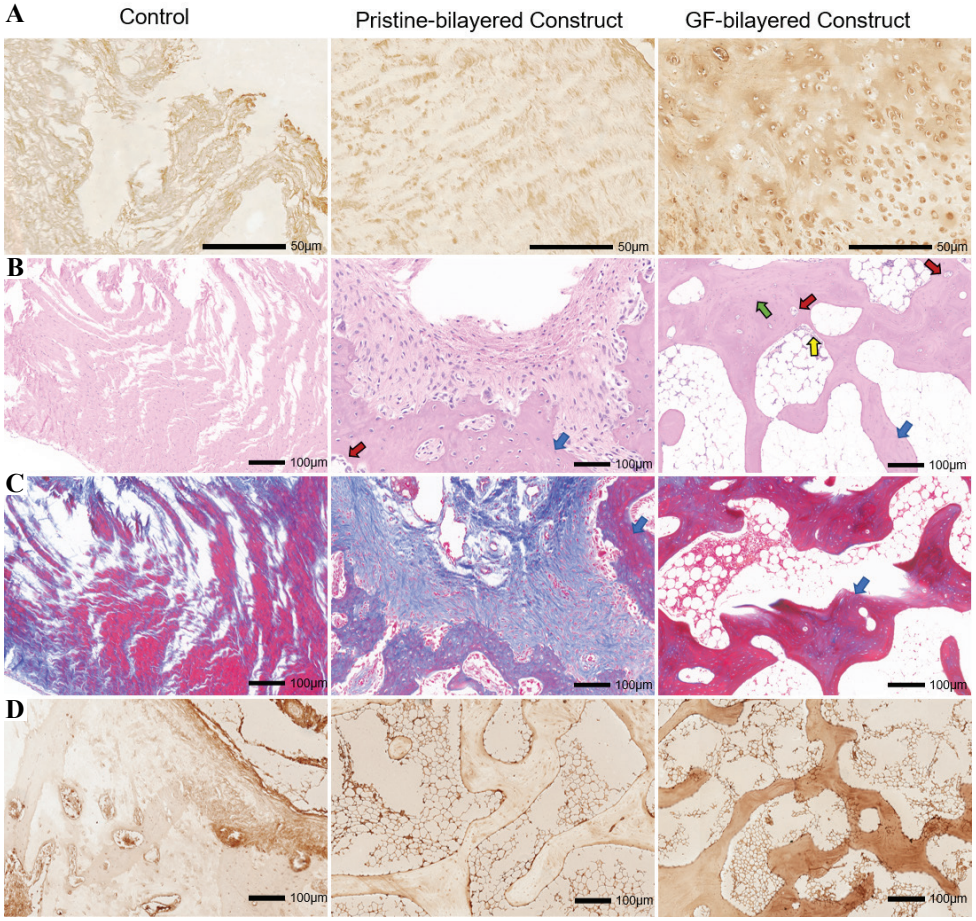

Figure 8. (A) Immunohistological staining for collagen type II of neocartilage at 3 months for the control group, pristine-bilayered construct group, and GF-bilayered construct group (scale bar: 50 μm). (B) H & E staining and imaging of neo-bone at high magnification at 3 months (blue arrows, trabecular structures; green arrows, typical osteoblasts; yellow arrows, osteocytes; red arrows, vascularization; scale bar: 100 μm). (C) Masson staining of neo-bone at 3 months (scale bar: 100 μm). (D) Immunohistological staining for OCN of neo-bone at 3 months (scale bar: 100 μm).

4. Conclusions

The present study has shown that each layer of scaffolds had a suitable mechanical strength and degradation rate. Furthermore, the scaffolds encapsulating TGF-β1 and BMP-2 can act as a controlled released system and promote directed differentiation of BMSCs. The *in vivo* experiments suggested that the scaffolds loaded with growth factors promoted osteochondral regeneration in the rabbit knee joint model. Altogether, the biomimetic bilayered scaffolds offer a novel option for application in osteochondral regeneration.

Acknowledgments

We would like to thank the Core Faility of Jiangsu Provincial People's Hospital for its help in the detection of experimental samples.

Funding

This work was supported by the National Natural Science Foundation of China (No. 81974332).

Conflicts of interest

There are no conflicts of interest to declare.

Authors' contributions

WM. F. planned the experiments; Q. Z. and Y. L. supervised the project; X. Z., ZX. L., R. X. and T. Y. carried out the experiments; Y. L. and Q. Z. performed the data analyses; X. Z. wrote the manuscript; QY. W., K. S., Y. Z., and K. Y. discussed the results, and reviewed and edited the manuscript.

References

1. Lewis PB, McCarty LP 3rd, Kang RW, et al., 2006, Basic Science and Treatment Options for Articular Cartilage Injuries. *J Orthop Sports Phys Ther*, 36:717–27.
2. Kilian D, Ahlfeld T, Akkineni AR, *et al*., 2020, 3D Bioprinting of Osteochondral Tissue Substitutes *in Vitro*-Chondrogenesis in Multi-layered Mineralized Constructs. *Sci Rep*, 10:8277.

3. Hu J, Zou WZ, Li L, *et al*., 2020, Overexpressing Runx2 of BMSCs Improve the Repairment of Knee Cartilage Defects. *Curr Gene Ther*, 20:395–404.
4. Stefani RM, Barbosa S, Tan AR, *et al*., 2002, Pulsed Electromagnetic Fields Promote Repair of Focal Articular Cartilage Defects with Engineered Osteochondral Constructs. *Biotechnol Bioeng*, 117:1584–96.
5. Levingstone TJ, Ramesh A, Brady RY, *et al*., 2016, Cell-free Multi-layered Collagen-based Scaffolds Demonstrate Layer Specific Regeneration of Functional Osteochondral Tissue in Caprine Joints. *Biomaterials*, 87:69–81.
6. Khanarian NT, Haney NM, Burga RA, *et al*., 2012, A Functional Agarose-hydroxyapatite Scaffold for Osteochondral Interface Regeneration. *Biomaterials*, 33:5247–58.
7. Abdollahiyan P, Oroojalian F, Mokhtarzadeh A, *et al*., 2002, Hydrogel-Based 3D Bioprinting for Bone and Cartilage Tissue Engineering. *Biotechnol J*, 2020:e2000095.
8. Abasalizadeh F, Moghaddam SV, Alizadeh E, *et al*., 2020, Alginate-based Hydrogels as Drug Delivery Vehicles in Cancer Treatment and their Applications in Wound Dressing and 3D Bioprinting. *J Biol Eng*, 14:8.
9. Zuo Q, Cui W, Liu F, *et al*., 2016, Utilizing Tissue-engineered Cartilage or BMNC-PLGA Composites to Fill Empty Spaces during Autologous Osteochondral Mosaicplasty in Porcine Knees. *J Tissue Eng Regen Med*, 10:916–26.
10. Cui W, Wang Q, Chen G, *et al*., 2011, Repair of Articular Cartilage Defects with Tissue-engineered Osteochondral Composites in Pigs. *J Biosci Bioeng*, 111:493–500.
11. Qiao Z, Lian M, Han Y, *et al*., 2021, Bioinspired Stratified Electrowritten Fiber-reinforced Hydrogel Constructs with Layer-specific Induction Capacity for Functional Osteochondral Regeneration. *Biomaterials*, 266:120385.
12. Cao R, Zhan A, Ci Z, *et al*., 2021, A Biomimetic Biphasic Scaffold Consisting of Decellularized Cartilage and Decalcified Bone Matrixes for Osteochondral Defect Repair. *Front Cell Dev Biol*, 9:639006.
13. Ashammakhi N, Ahadian S, Xu C, *et al*., 2019, Bioinks and Bioprinting Technologies to Make Heterogeneous and Biomimetic Tissue Constructs. *Mater Today Bio*, 1:100008.
14. Antich C, de Vicente J, Jimenez G, *et al*., 2002, Bio-inspired Hydrogel Composed of Hyaluronic Acid and Alginate as a Potential Bioink for 3D Bioprinting of Articular Cartilage Engineering Constructs. *Acta Biomater*, 106:114–23.
15. Zhang W, Ling C, Zhang A, *et al*., 2020, An All-silk-derived Functional Nanosphere Matrix for Sequential Biomolecule Delivery and *In Situ* Osteochondral Regeneration. *Bioact Mater*, vol. 5, no. 4, pp. 832-843, 2020.
16. Ng WL, Chua CK, Shen YF, 2019, Print Me An Organ! Why We Are Not There Yet. *Prog Polym Sci*, 97:101145.
17. Liu N, Ye X, Yao B, *et al*., 2021, Advances in 3D Bioprinting Technology for Cardiac Tissue Engineering and Regeneration. *Bioact Mater*, 6:1388–401.
18. Osidak EO, Kozhukhov VI, Osidak MS, *et al*., 2020, Collagen as Bioink for Bioprinting: A Comprehensive Review. *Int J Bioprint*, 6:270.
19. Lee JM, Sing SL, Yeong WY, 2002, Bioprinting of Multimaterials with Computer-aided Design/Computer-aided Manufacturing. *Int J Bioprint*, 6:245.
20. Gantumur E, Nakahata M, Kojima M, *et al*., 2002, Extrusion-Based Bioprinting through Glucose-Mediated Enzymatic Hydrogelation. *Int J Bioprint*, 6:250.
21. Askari M, Naniz MA, Kouhi M, *et al*., 2020, Recent Progress in Extrusion 3D Bioprinting of Hydrogel Biomaterials for Tissue Regeneration: A Comprehensive Review with Focus on Advanced Fabrication Techniques. *Biomater Sci*, 9:535–573.
22. Li X, Liu B, Pei B, *et al*., 2020, Inkjet Bioprinting of Biomaterials. *Chem Rev*, 120:10793–833.
23. Ng WL, Lee JM, Zhou M, *et al*., 2002, Vat Polymerization-based Bioprinting-process, Materials, Applications and Regulatory Challenges. *Biofabrication*, 12:022001.
24. Vurat MT, Ergun C, Elcin AE, *et al*., 2002, 3D Bioprinting of Tissue Models with Customized Bioinks. *Adv Exp Med Biol*, 1249:67–84.
25. Ning L, Mehta R, Cao C, *et al*., 2020, Embedded 3D Bioprinting of Gelatin Methacryloyl-Based Constructs with Highly Tunable Structural Fidelity. *ACS Appl Mater Interfaces*, 12:44563–577.
26. Bicho D, Ajami S, Liu C, *et al*., 2019, Peptide-biofunctionalization of Biomaterials for Osteochondral Tissue Regeneration in Early Stage Osteoarthritis: Challenges and Opportunities. *J Mater Chem B*, 7:1027–44.
27. Gan D, Xu T, Xing W, *et al*., 2019, Mussel-inspired Dopamine Oligomer Intercalated tough and Resilient Gelatin Methacryloyl (GelMA) Hydrogels for Cartilage Regeneration. *J Mater Chem B*, 7:1716–25.
28. Mishbak HH, Cooper G, Bartolo PJ, 2019, Development and Characterization of a Photocurable Alginate Bioink for Three-dimensional Bioprinting. *Int J Bioprint*, 5:189.
29. Chang R, Nam J, Sun W, 2008, Effects of Dispensing Pressure and Nozzle Diameter on Cell Survival from Solid Freeform Fabrication-based Direct Cell Writing. *Tissue Eng Part A*, 14:41–8.
30. Pati F, Jang J, Ha DH, *et al*., 2014, Printing Three-dimensional Tissue Analogues with Decellularized Extracellular Matrix

Bioink. *Nat Commun*, 5:3935.

31. Fedorovich NE, De Wijn JR, Verbout AJ, *et al*., 2008, Three-dimensional Fiber Deposition of Cell-laden, Viable, Patterned Constructs for Bone Tissue Printing. *Tissue Eng Part A*, 14:127–33.
32. Abaci A, Guvendiren M, 202, Designing Decellularized Extracellular Matrix-Based Bioinks for 3D Bioprinting. *Adv Healthc Mater*, 2020:e2000734.
33. Shin YJ, Shafranek RT, Tsui JH, *et al*., 3D Bioprinting of Mechanically Tuned Bioinks Derived from Cardiac Decellularized Extracellular Matrix. *Acta Biomater*, 1;119:75–88.
34. Lee H, Yang GH, Kim N, *et al*., 2018, Fabrication of Micro/Nanoporous Collagen/dECM/Silk-fibroin Biocomposite Scaffolds Using a Low Temperature 3D Printing Process for Bone Tissue Regeneration. *Mater Sci Eng C Mater Biol Appl*, 84:140–7.
35. Yang Q, Peng J, Guo Q, *et al*., 2008, A Cartilage ECM-derived 3-D Porous Acellular Matrix Scaffold for *In Vivo* Cartilage Tissue Engineering with PKH26-labeled Chondrogenic Bone Marrow-derived Mesenchymal Stem Cells. *Biomaterials*, 29:2378–87.
36. Jang J, Kim TG, Kim BS, *et al*., 2016, Tailoring Mechanical Properties of Decellularized Extracellular Matrix Bioink by Vitamin B2-Induced Photo-Crosslinking. *Acta Biomaterialia*, 33:88–95.
37. Zhang X, Liu Y, Luo C, *et al*., 2002, Crosslinker-free Silk/Decellularized Extracellular Matrix Porous Bioink for 3D Bioprinting-based Cartilage Tissue Engineering. *Mater Eng C*, 2020:111388.
38. Li Z, Zhang X, Yuan T, *et al*., 2020, Addition of Platelet-Rich Plasma to Silk Fibroin Hydrogel Bioprinting for Cartilage Regeneration. *Tissue Eng Part A*, 26:886–95.
39. Gupta S, Alrabaiah H, Christophe M, *et al*., 2020, Evaluation of Silk-based Bioink during Pre and Post 3D Bioprinting: A Review. *J Biomed Mater Res B Appl Biomater*, 109:279–93.
40. Almeida HV, Liu Y, Cunniffe GM, *et al*., 2014, Controlled Release of Transforming Growth Factor-beta3 from Cartilage-extra-cellular-matrix-derived Scaffolds to Promote Chondrogenesis of Human-joint-tissue-derived Stem Cells. *Acta Biomater*, 10:4400–9.
41. Almeida HV, Cunniffe GM, Vinardell T, *et al*., 2015, Coupling Freshly Isolated CD44(+) Infrapatellar Fat Pad-Derived Stromal Cells with a TGF-beta3 Eluting Cartilage ECM-Derived Scaffold as a Single-Stage Strategy for Promoting Chondrogenesis. *Adv Healthc Mater*, 4:1043–53.
42. Dickman CT, Russo V, Thain K, *et al*., 2002, Functional Characterization of 3D Contractile Smooth Muscle Tissues Generated Using a Unique Microfluidic 3D Bioprinting Technology. *FASEB J*, 34:1652–64.
43. Stanco D, Boffito M, Bogni A, *et al*., 2002, 3D Bioprinting of Human Adipose-Derived Stem Cells and Their Tenogenic Differentiation in Clinical-Grade Medium. *Int J Mol Sci*, 21:8694.
44. Sawkins MJ, Bowen W, Dhadda P, *et al*., 2013, Hydrogels Derived from Demineralized and Decellularized Bone Extracellular Matrix. *Acta Biomater*, 9:7865–73.
45. Zhang X, Zhai C, Fei H, *et al*., 2018, Composite Silk-Extracellular Matrix Scaffolds for Enhanced Chondrogenesis of Mesenchymal Stem Cells. *Tissue Eng Part C Methods*, 24:645–58.
46. Chenjun Z, Qiang Z, Kai S, *et al*., 2002, Utilizing an Integrated Tri-layered Scaffold with Titanium-Mesh-Cage Base to Repair Cartilage Defects of Knee in Goat Model. *Mater Des*, 193:108766.
47. Zhai C, Fei H, Hu J, *et al*., 2018, Repair of Articular Osteochondral Defects Using an Integrated and Biomimetic Trilayered Scaffold. *Tissue Eng Part A*, 24:1680–92.
48. Crapo PM, Gilbert TW, Badylak SF, 2011, An Overview of Tissue and Whole Organ Decellularization Processes. *Biomaterials*, 32:3233–43.
49. Schacht K, Jungst T, Schweinlin M, *et al*., 2015, Biofabrication of Cell-loaded 3D Spider Silk Constructs. *Angew Chem Int Ed Engl*, 54:2816–20.
50. Ni T, Liu M, Zhang Y, *et al*., 2002, 3D Bioprinting of Bone Marrow Mesenchymal Stem Cell-Laden Silk Fibroin Double Network Scaffolds for Cartilage Tissue Repair. *Bioconjug Chem*, 31:1938–47.
51. Chawla S, Midha S, Sharma A, *et al*., 2018, Silk-Based Bioinks for 3D Bioprinting. *Adv Healthc Mater*, 7:e1701204.
52. Ding C, Qiao Z, Jiang W, *et al*., 2013, Regeneration of a Goat Femoral Head Using a Tissue-specific, Biphasic Scaffold Fabricated with CAD/CAM Technology. *Biomaterials*, 34:6706–16.
53. Cals FL, Hellingman CA, Koevoet W, *et al*., 2012, Effects of Transforming Growth Factor-beta Subtypes on *In Vitro* Cartilage Production and Mineralization of Human Bone Marrow Stromal-derived Mesenchymal Stem Cells. *J Tissue Eng Regen Med*, 6:68–76.
54. Freeman FE, Pitacco P, van Dommelen LH, *et al*., 2002, 3D Bioprinting Spatiotemporally Defined Patterns of Growth Factors to Tightly Control Tissue Regeneration. *Sci Adv*, 6:eabb5093.
55. Datta S, Rameshbabu AP, Bankoti K, *et al*., 2021,

Decellularized Bone Matrix/Oleoyl Chitosan Derived Supramolecular Injectable Hydrogel Promotes Efficient Bone Integration. *Mater Sci Eng C Mater Biol Appl*, 119:111604.

56. Das S, Pati F, Chameettachal S, *et al*., 2013, Enhanced Redifferentiation of Chondrocytes on Microperiodic Silk/Gelatin Scaffolds: Toward Tailor-made Tissue Engineering. *Biomacromolecules*, 14:311–21.
57. Huh JE, Koh PS, Seo BK, *et al*., 2014, Mangiferin Reduces the Inhibition of Chondrogenic Differentiation by IL-1beta in Mesenchymal Stem Cells from Subchondral Bone and Targets Multiple Aspects of the Smad and SOX9 Pathways. *Int J Mol Sci*, 15:16025–42.